Electronic Supplementary Information

Increase the Molecular Length and Donor Strength to Boost Horizontal Dipole Orientation for High-efficiency OLEDs

Yi-Kuan Chen,[a+] Jayachandran Jayakumar,[a+] Chang-Lun Ko,[c] Wen-Yi Hung,[c] Tien-Lin Wu,*[,a] Chien-Hong Cheng*[,ab]

E-mail: tlwu@mx.nthu.edu.tw
E-mail: chcheng@mx.nthu.edu.tw

[a]Department of Chemistry, National Tsing Hua University No. 101, Sec. 2, Kuang-Fu Rd., Hsinchu 30013, Taiwan
[b]Department of Chemistry, National Sun Yat-sen University, Kaohsiung, 80424, Taiwan
[c]Institute of Optoelectronic Sciences, National Taiwan Ocean University, Keelung 20224, Taiwan.

Keywords: molecular length, spiroacridine; TADF; horizontal dipole orientation; organic electronics; organic light-emitting diode

Table of Contents **Page No**

General Information

All chemicals and reagents were purchased from commercial providers without further purification. ^{1}H NMR and ^{13}C NMR spectra were measured on a Varian INOVA-500 NMR spectrometer. Mass spectra were performed on JEOL AccuTOF GCx HRGCMS and JEOL JMS-700 HRMS. Elemental analyses were performed using an analyzer (Vario EL III CHN-OS Rapid, Elementar). UV-vis absorption spectra were recorded on a Hitachi U-3300 spectrophotometer. Fluorescence and Phosphorescence spectra were recorded on a Hitachi F-7000 fluorescence spectrophotometer. The absolute photoluminescence quantum efficiencies (PLQYs) of the doped films were determined using an integrating sphere under an N_2 atmosphere. The thermogravimetric analysis (TGA) and differential scanning calorimetry (DSC) were performed on a thermal analyzer (2-HT, Mettler-Toledo) at a heating rate of 10 °C/min. from 30 °C to 800 °C under nitrogen. Transient PL decay measurements were done using an Edinburgh FLS 980 instrument. The HOMO levels of emitters in the neat film were determined by a Riken Keiki AC-2 photoelectron spectrometer with a UV source. The X-ray diffraction was carried out on an X-ray diffractometer (X8 APEX, Bruker). The measurement of horizontal dipoles ratios uses a 10 kHz, 355-nm Nd: YAG Laser as the continuous excitation source, a polarizer, and a spectrometer (Ocean Optics USB4000) to collect the PL spectra, and the results were fitted by SETFOS 4.5 software.

Chemicals. All starting materials, ammonium acetate, benzoylacetonitriles, and their derivatives were purchased from commercial suppliers unless otherwise mentioned.

Theoretical Calculation. Molecular geometry optimizations and electronic properties of these materials were carried out by using the Gaussian 09 program with density functional theory (DFT) and time-dependent DFT (TD-DFT for S_1 and T_n states) calculations in which the Perdew-Burke-Ernzerhof (PBE0) hybrid exchange-correlation functional with the 6-31G(d) basis set was used. [1, 2] The molecular orbitals were visualized by Gaussview 5.0 software. All calculations were performed in the gas phase.

Experimental

Syntheses of starting materials.

Synthesis of 4-(9*H*-carbazol-9-yl)-2,6-dimethylbenzaldehyde:

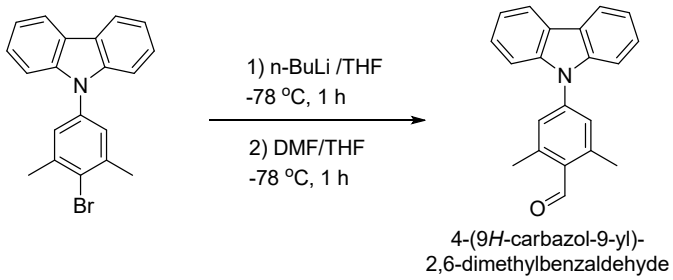

n-Butyllithium (1.7 mL, 4.3 mmol) was added dropwise to a solution of 9-(4-bromo-3,5-dimethylphenyl)-9*H*-carbazole (1.0 g, 2.9 mmol) in anhydrous THF (19 mL, 0.15 M) and remained at -78 °C for 1 h. Anhydrous DMF (0.6 g, 8.7 mmol) was slowly added and kept at -78 °C for another 1 h. After overnight reaction at room temperature, the mixture was extracted with ethylacetate/water, dried over anhydrous Na_2SO_4, and treated with reduced pressure to remove the solvent. The crude product was purified by column chromatography using ethyl acetate/hexane (1:19, v/v) as eluent to give the desired product as yellow solid (0.7 g, yield: 80 %). **^{1}H NMR (500 MHz, $CDCl_3$, δ):** 10.67 (s, 1H), 8.12 (d, *J* = 8.0 Hz, 2H), 7.48 (d, *J* = 8.5 Hz, 2H), 7.42 (t, *J* = 8.0 Hz, 2H), 7.34 (s, 2H), 7.30 (t, *J* = 7.5 Hz, 2H), 2.72 (s, 6H). **^{13}C NMR (125 MHz, $CDCl_3$, δ):** 192.41, 143.51, 141.58, 140.11, 130.91, 127.17, 126.13, 123.79, 120.52, 120.43, 109.92, 20.80.

Synthesis of 4-(3,6-di-*tert*-butyl-9*H*-carbazol-9-yl)-2,6-dimethylbenzaldehyde:

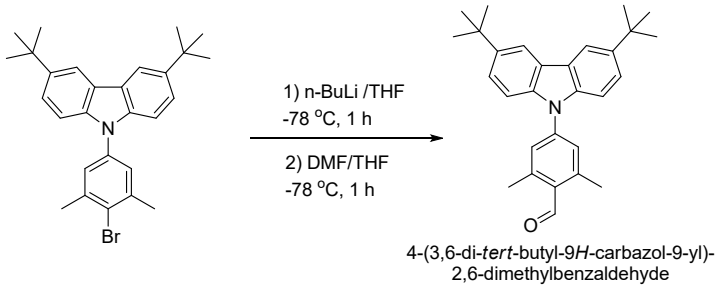

4-(3,6-di-tert-butyl-9*H*-carbazol-9-yl)-2,6-dimethylbenzaldehyde was synthesized by a similar procedure as 4-(9*H*-carbazol-9-yl)-2,6-dimethylbenzaldehyde. n-Butyllithium (1.3 mL, 3.1 mmol) was added dropwise to a solution of 9-(4-bromo-3,5-dimethylphenyl)-3,6-di-tert-butyl-9*H*-

carbazole (1.0 g, 2.2 mmol) in anhydrous THF (14 mL, 0.15 M) at -78 °C for 1 h. Anhydrous DMF (0.5 g, 6.5 mmol) was slowly added and kept at -78 °C for another 1 h. After overnight reaction at room temperature, the mixture was extracted with ethylacetate/water, dried over anhydrous Na_2SO_4, and reduced pressure to remove the solvent. The crude product was purified by column chromatography using ethyl acetate/hexane (1:19, v/v) as eluent to give the desired product as yellow solid (0.6 g, yield: 67 %). **^{1}H NMR (500 MHz, $CDCl_3$, δ):** 10.66 (s, 1H), 8.12 (s, 2H), 7.47 (d, *J* = 8.5 Hz, 2H), 7.44 (d, *J* = 8.5 Hz, 2H), 7.33 (s, 2H), 2.71 (s, 6H), 1.45 (s, 18H). **^{13}C NMR (125 MHz, $CDCl_3$, δ):** 192.34, 143.56, 143.47, 142.13, 138.38, 130.39, 126.58, 123.87, 123.78, 116.37, 109.44, 34.75, 31.95, 20.84.

Synthesis of 2,6-dimethyl-4-(10*H*-spiro[acridine-9,9'-fluoren]-10-yl)benzaldehyde:

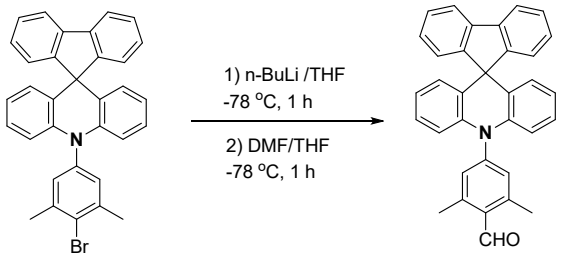

2,6-dimethyl-4-(10*H*-spiro[acridine-9,9'-fluoren]-10-yl)benzaldehyde

2,6-Dimethyl-4-(10*H*-spiro[acridine-9,9'-fluoren]-10-yl)benzaldehyde was synthesized by a similar procedure as 4-(9*H*-carbazol-9-yl)-2,6-dimethylbenzaldehyde. n-Butyllithium (1.2 mL, 2.9 mmol) was added dropwise to a solution of 10-(4-bromo-3,5-dimethylphenyl)-10*H*-spiro[acridine-9,9'-fluorene] (1.0 g, 1.9 mmol) in anhydrous THF (24 mL, 0.08 M) at -78 °C for 1 h. Anhydrous DMF (4.3 g, 5.7 mmol) was slowly added and kept at -78 °C for another 1 h. After overnight reaction at room temperature, the mixture was extracted with ethylacetate/water, dried over anhydrous Na_2SO_4, and reduced pressure to remove the solvent. The crude product was purified by column chromatography using ethyl acetate/hexane (1:19, v/v) as eluent to give the desired product as yellow solid (0.6 g, yield: 67 %). **^{1}H NMR (500 MHz, $CDCl_3$, δ):** 10.72 (s, 1H), 7.77 (d, *J* = 7.5 Hz, 2H), 7.38-7.33 (m, 4H), 7.23-7.21 (m, 4H), 6.90 (t, *J* = 7.5 Hz, 2H), 6.55 (t, *J* = 7.5 Hz, 2H), 6.38 (d, *J* = 7.5 Hz, 2H), 6.34 (d, *J* = 7.5 Hz, 2H), 2.72 (s, 6H). **^{13}C NMR (125 MHz, $CDCl_3$, δ):** 192.87, 156.52, 144.96, 144.44, 140.59, 139.19, 132.40, 132.13, 128.37, 127.96, 127.62, 127.23, 125.72, 124.80, 120.86, 119.91, 114.46, 20.67.

Synthesis of 4-(4-(9*H*-carbazol-9-yl)-2,6-dimethylphenyl)-2,6-diphenylpyridine-3,5-

dicarbonitrile (CzmPPC):

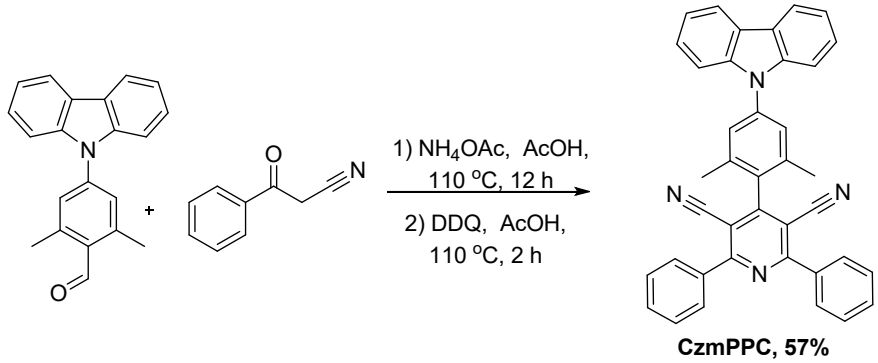

CzmPPC, 57%

To a mixture of 4-(9*H*-carbazol-9-yl)-2,6-dimethylbenzaldehyde (0.7 g, 2.2 mmol), benzoyl acetonitrile (0.8 g, 5.6 mmol) and ammonium acetate (0.4 g, 5.6 mmol), acetic acid (7 mL) were added and refluxed for 12 h. After cooling to room temperature, a homogeneous solution of DDQ (1.4 g, 6.4 mmol) was added and stirred for 2 h at 110 ºC. The reaction was quenched with water, and the mixture was filtered. The crude product was purified by column chromatography using dichloromethane/hexane (1:1, v/v) as eluent to give the desired product as yellow solid (1.5 g, yield: 57 % and the overall yield: 46%). **^{1}H NMR (500 MHz, $CDCl_3$, δ):** 8.19-8.15 (m, 6H), 7.62-7.61 (m, 6H), 7.55 (d, *J* = 8.0 Hz, 2H), 7.51 (s, 2H), 7.46 (t, *J* = 8.0 Hz, 2H), 7.31 (t, *J* = 7.5 Hz, 2H), 2.31 (s, 6H). **^{13}C NMR (125 MHz, $CDCl_3$, δ):** 163.12, 160.71, 140.56, 139.36, 137.12, 136.06, 132.50, 131.68, 129.52, 128.91, 126.75, 126.04, 123.50, 120.28, 120.15, 115.05, 110.01, 106.45, 20.29. HRMS (FD) m/z: [M+] calcd. for $C_{39}H_{26}N_4$, 550.2152; found, 550.2151. Elemental Anal. calcd. for $C_{39}H_{26}N_4$: C 85.07, H 4.76, N 10.17 found: C 85.17, H 4.51, N 10.03.

Synthesis of 4-(4-(3,6-di-tert-butyl-9*H*-carbazol-9-yl)-2,6-dimethylphenyl)-2,6-diphenylpyridine-3,5-dicarbonitrile (tCzmPPC):

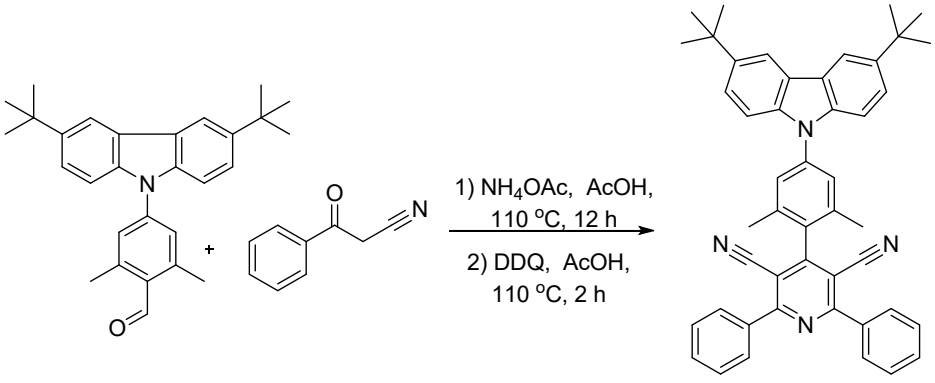

tCzmPPC, 68%

To a mixture of 4-(3,6-di-tert-butyl-9*H*-carbazol-9-yl)-2,6-dimethylbenzaldehyde (0.2 g, 0.5

mmol), benzoylacetonitrile (0.2 g, 1.2 mmol), ammonium acetate (0.1 g, 1.5 mmol), and acetic acid (5 mL) were added and refluxed for 12 h. After cooling to room temperature, a homogeneous solution of DDQ (0.2 g, 2.5 mmol) was added and stirred for 2 h at 110 °C. The reaction was quenched with water, and the mixture was filtered. The crude product was purified by column chromatography using dichloromethane/hexane (1:1, v/v) as eluent to give the desired product as orange-yellow solid (0.4 g, yield: 68 % and the overall yield: 46%). **^{1}H NMR (500 MHz, $CDCl_3$, δ):** 8.15-8.13 (m, 6H), 7.60 (m, 6H), 7.48 (m, 6H), 2.27 (s, 6H), 1.46 (s, 18H). **^{13}C NMR (125 MHz, $CDCl_3$, δ):** 163.10, 160.84, 143.10, 139.89, 138.89, 136.92, 136.11, 131.90, 131.65, 129.53, 128.91, 126.24, 123.69, 123.54, 116.20, 115.06, 109.49, 106.57, 34.73, 31.99, 20.29. HRMS (EI) m/z: [M+] calcd. for $C_{47}H_{42}N_4$, 662.3404; found, 662.3405. Elemental Anal. calcd. for $C_{47}H_{44}N_4$: C 85.16, H 6.39, N 8.45 found: C 85.56, H 5.98, N 8.51.

Synthesis of 4-(2,6-dimethyl-4-(10*H*-spiro[acridine-9,9'-fluoren]-10-yl)phenyl)-2,6-diphenylpyridine-3,5-dicarbonitrile (SAcmPPC):

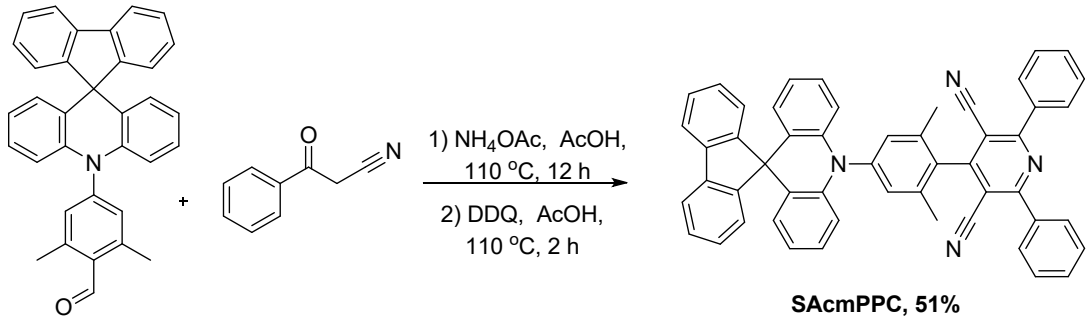

To a mixture of 2,6-dimethyl-4-(10*H*-spiro[acridine-9,9'-fluoren]-10-yl)benzaldehyde (0.2 g, 0.4 mmol), benzoylacetonitrile (0.2 g, 1.1 mmol), ammonium acetate (0.1 g, 1.3 mmol), and acetic acid (6 mL) were added and refluxed for 12 h. After cooling to room temperature, a homogeneous solution of DDQ (1.0 g, 0.2 mmol) was added and stirred for 2 h at 110 °C. The reaction was quenched with water, and the mixture was filtered. The crude product was purified by column chromatography using dichloromethane/hexane (1:1, v/v) as eluent to give the desired product as orange-yellow solid (0.3 g, yield: 51 % and the overall yield: 34%). **^{1}H NMR (500 MHz, $CDCl_3$, δ):** 8.19 (d, *J* = 7.5 Hz, 4H), 7.79 (d, *J* = 7.5 Hz, 2H), 7.62-7.61 (m, 6H), 7.43-7.42 (m, 4H), 7.37 (t, *J* = 7.5 Hz, 2H), 7.26 (d, *J* = 7.5 Hz, 2H), 6.98 (t, *J* = 7.5 Hz, 2H), 6.58 (t, *J* = 7.5 Hz, 2H), 6.49 (d, *J* = 8.5 Hz, 2H), 6.41 (d, *J* = 8.0 Hz, 2H), 2.33 (s, 6H). **^{13}C NMR (125 MHz, $CDCl_3$, δ):** 163.09, 160.88, 156.52, 142.69, 140.93, 139.21, 138.48, 136.07, 133.97, 131.74, 131.10, 129.55, 129.53, 128.95, 128.35, 127.73, 127.57, 127.48, 125.77, 124.75, 120.76, 119.88, 115.06, 114.67,

106.37, 20.27. HRMS (EI) m/z: [M+] calcd. for $C_{52}H_{34}N_4$, 714.2778; found, 714.2773. Elemental Anal. calcd. for $C_{52}H_{34}N_4$: C 87.37, H 4.79, N 7.84 found: C 87.56, H 4.38, N 7.91.

OLEDs Fabrication and Measurement. Organic materials used in device fabrication were purified by sublimation. Devices were fabricated by vacuum deposition onto pre-coated ITO glass with a sheet resistance of 25 Ω/square at a pressure lower than 10^{-6} Torr. Organic materials were deposited at the rate of 0.5~1.2 Å s^{-1}. LiF and Al were deposited at the rate of 0.1 Å s^{-1} and 3~10 Å s^{-1}, respectively. The rest of the procedures is similar to the reported method. Current-voltage-luminance (I-V-L) characterization and electroluminescent spectra were measured and recorded by using a programmable source meter (2400, Keithley) and a spectroradiometer (CS2000A, Konica Minolta). The Lambertian emission assumption determined external quantum efficiencies and power efficiencies. All devices were encapsulated in a glove box. Then, the EL measurements were performed at room temperature.

.

Table S1. Singlet and triplet excitation states, and transition configurations of CzmPPC by TD-DFT at the PBE0/6-31G (d).

State	Excitation		E_{cal} (eV)[a]	λ_{cal} (nm)[b]	f[c]
	Singlet Excited States				
S_1	HOMO→LUMO	0.70486	2.7164	456.43	0.0003
S_2	HOMO→LUMO+1	0.69991	3.0681	404.15	0.0407
S_3	HOMO-1→LUMO	0.70698	3.1679	391.37	0.0000
S_4	HOMO-1→ LUMO+1	0.70514	3.5509	349.17	0.0001
S_5	HOMO-10→LUMO	0.16488	3.9962	310.25	0.5420
	HOMO-2→LUMO	0.64362			
	HOMO→LUMO+2	0.19125			
	Triplet Excited States				
T_1	HOMO-10→LUMO	-0.10565	2.6481	468.20	0.0000
	HOMO-11→LUMO+1	-0.15569			
	HOMO-6→LUMO+1	-0.10565			
	HOMO-5→LUMO+1	-0.12425			
	HOMO-2→LUMO	0.61016			
T_2	HOMO→LUMO	0.70374	2.7106	457.41	0.0000
T_3	HOMO-5→LUMO+1	-0.10785	2.7136	415.80	0.0000
	HOMO-5→LUMO+2	-0.11246			
	HOMO→LUMO+1	0.63431			
	HOMO→LUMO+2	-0.18221			

[a]Excitation energy, [b]excitation wavelength (λ), [c]oscillator strength (*f*).

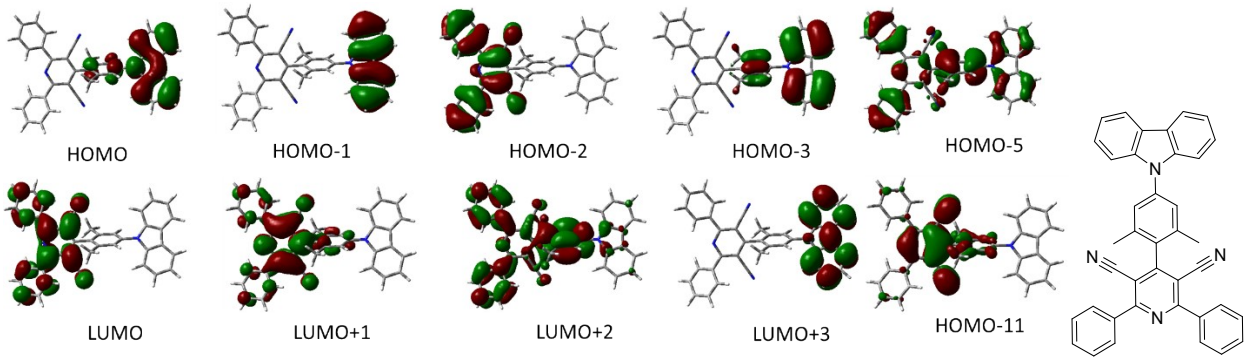

Table S2. Singlet and triplet excitation states, and transition configurations of the tCzmPPC by TD-DFT at the PBE0/6-31G (d).

State	Excitation		E_{cal} (eV)[a]	λ_{cal} (nm)[b]	f[c]
	Singlet Excited States				
S_1	HOMO→LUMO	0.70503	2.5647	483.43	0.0002
S_2	HOMO→LUMO+1	0.70064	2.9323	422.83	0.0367
S_3	HOMO-1→LUMO	0.70694	3.0767	402.97	0.0000
S_4	HOMO-1→LUMO	0.70538	3.4732	356.97	0.0002
S_5	HOMO-4→LUMO	-0.11180	3.9627	312.88	0.6435
	HOMO-3→LUMO	0.46940			
	HOMO-2→LUMO	-0.14191			
	HOMO→LUMO+2	0. 43835			
	HOMO→LUMO+4	0.19648			
	HOMO→LUMO+3	0.16961			
	Triplet Excited States				
T_1	HOMO→LUMO	0.70433	2.5598	484.34	0.0000
T_2	HOMO-12→LUMO	-0.13931	2.6491	468.02	0.0000
	HOMO-11→LUMO+1	-0.15320			
	HOMO-6→LUMO+1	-0.13181			
	HOMO-3→LUMO	0.61239			
T_3	HOMO→LUMO+1	0.66047	2.8744	431.34	0.0000
	HOMO→LUMO+2	-0.15072			

[a]Excitation energy, [b]excitation wavelength (λ), [c]oscillator strength (*f*).

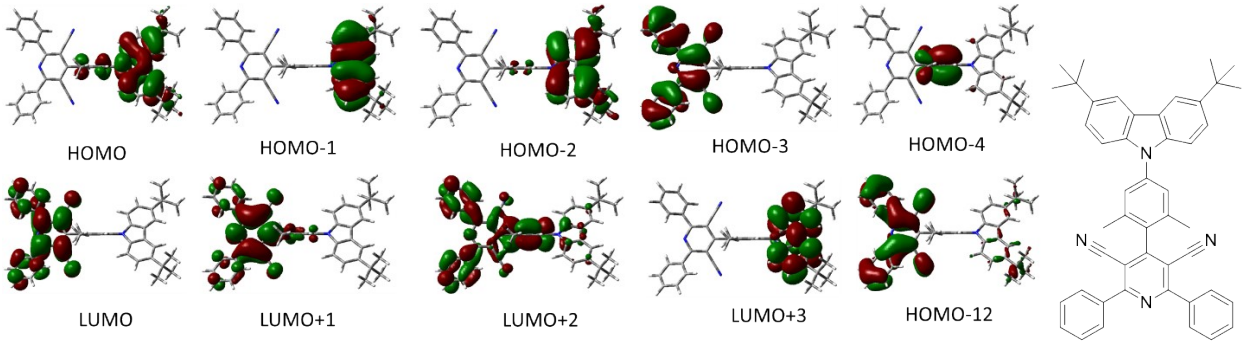

Table S3. Singlet and triplet excitation states, and transition configurations of the SAcmPPC by TD-DFT at the PBE0/6-31G (d).

State	Excitation		E_{cal} (eV)[a]	λ_{cal} (nm)[b]	f[c]
	Singlet Excited States				
S_1	HOMO→LUMO	0.70687	2.2298	556.04	0.0000
S_2	HOMO→LUMO+1	0.70588	2.6504	467.79	0.0007
S_3	HOMO-1→LUMO	0.70597	3.0797	402.59	0.0000
S_4	HOMO→LUMO+2	0.69721	3.4932	354.93	0.0012
S_5	HOMO-1→LUMO+1	0.70528	3.5242	351.80	0.0000
	Triplet Excited States				
T_1	HOMO→LUMO	0.70685	2.2297	556.07	0.0000
T_2	HOMO-6→LUMO	0.23774	2.6488	468.07	0.0000
	HOMO→LUMO+1	0.65098			
T_3	HOMO-16→LUMO	0.13377	2.6518	467.55	0.0000
	HOMO-15→LUMO+1	0.14069			
	HOMO-10→LUMO+1	-0.14454			
	HOMO-6→LUMO	0.56774			
	HOMO→LUMO+1	-0.27275			

[a]Excitation energy, [b]excitation wavelength (λ), [c]oscillator strength (*f*).

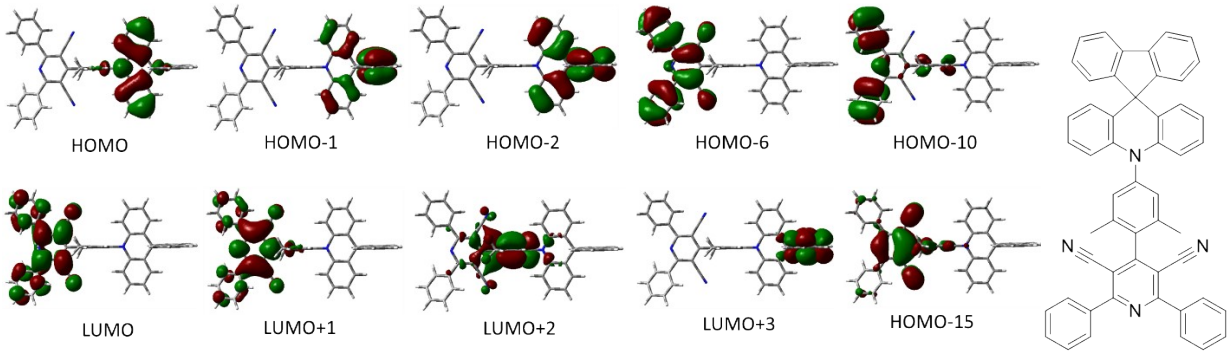

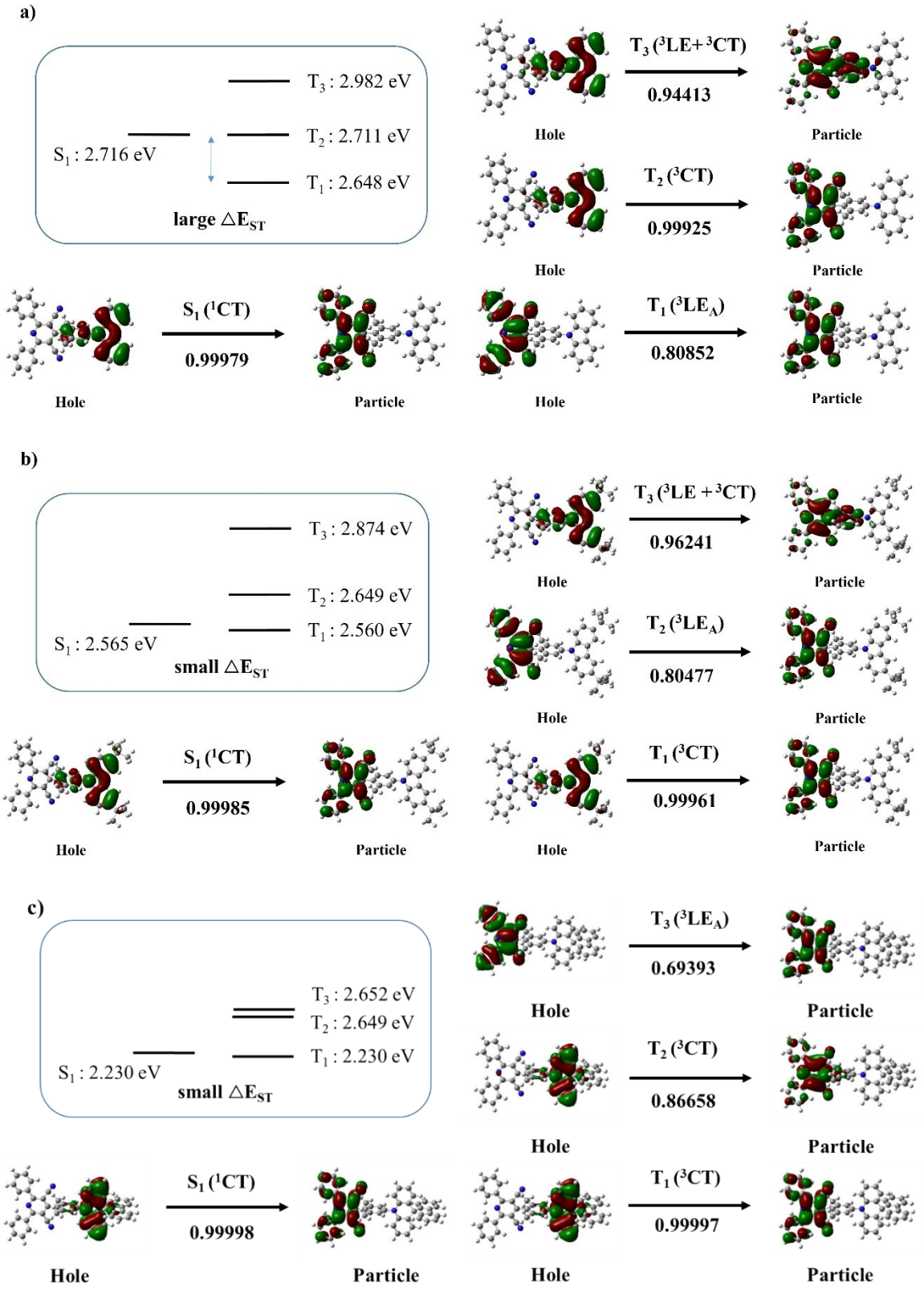

Figure S1. Natural transition orbitals characteristics of S_1 and T_n excited states of a) CzmPPC, b) tCzmPPC, and c) SAcmPPC.

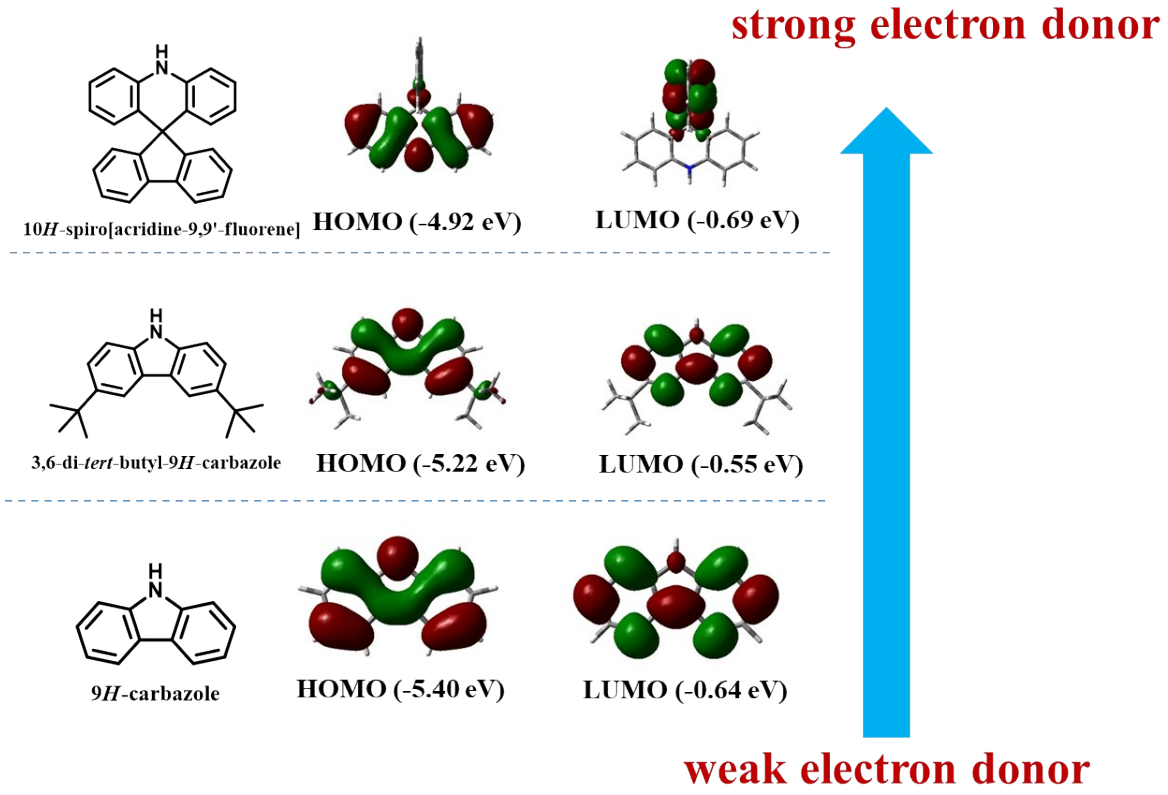

Figure S2. The chemical structures and the optimized geometries with molecular orbitals of spiroacridine, *tert*-butyl-carbazole, and carbazole.

Photophysical properties

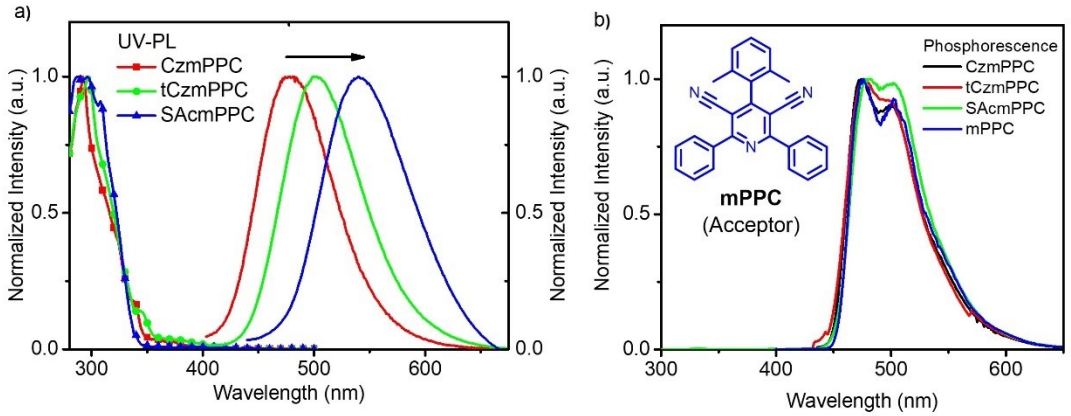

Figure S3. a) UV-vis spectra and PL spectra of CzmPPC, tCzmPPC, and SAcmPPC at RT b) Phosphorescence spectra of CzmPPC, tCzmPPC, SAcmPPC and the acceptor (mPPC) at LT in toluene (10^{-5} M).

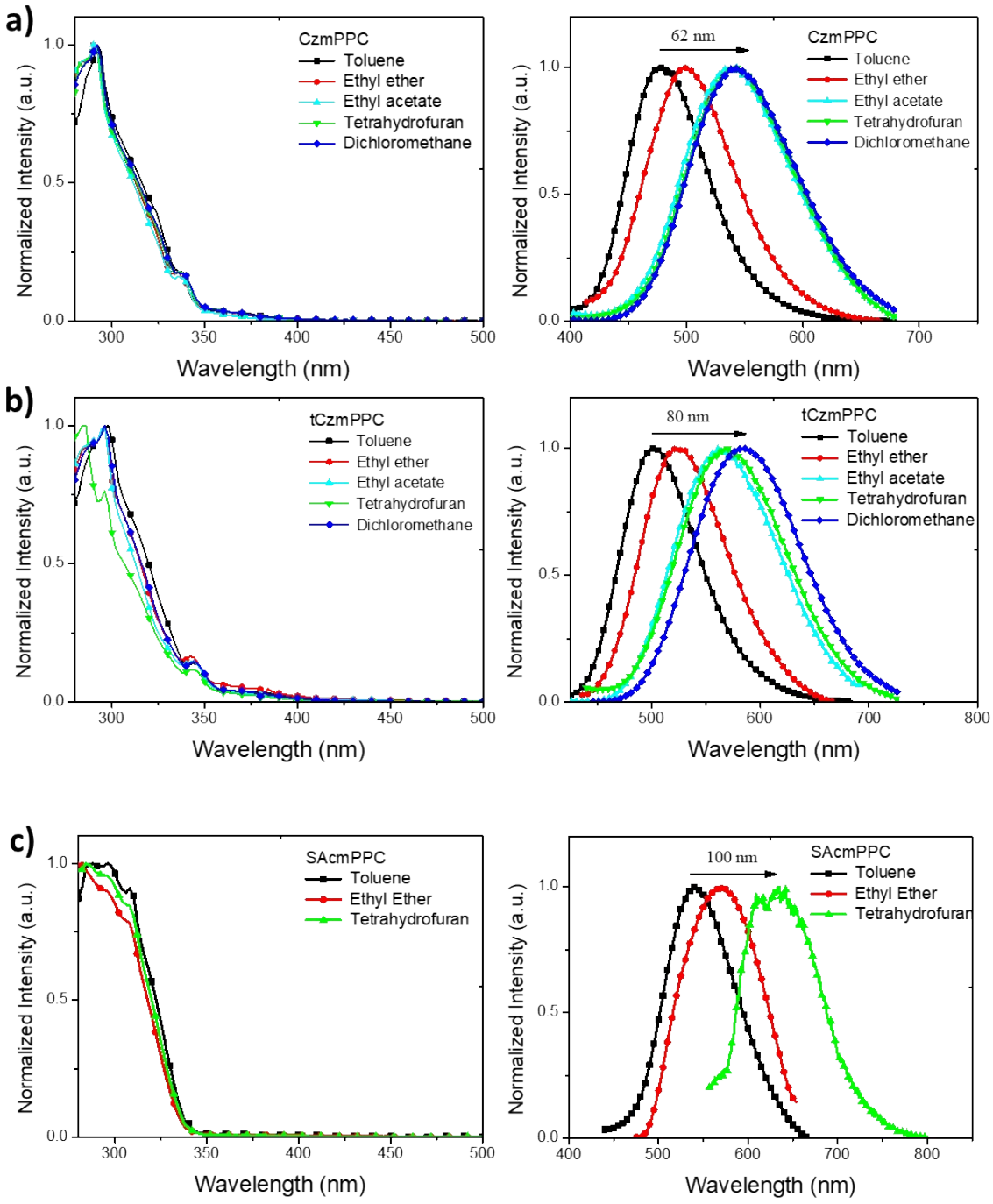

Figure S4. UV-vis and PL-spectra of a) CzmPPC, b) tCzmPPC, and c) SAcmPPC, respectively, in various solvents at RT (10^{-5} M).

Table S4. The photophysical and thermal data of these three emitters.

emitter	S_1 (eV)[a/b]	T_1 (eV)[c/d]	E_g (eV)[e]	T_m (°C)[f]
CzmPPC	2.92/2.95	2.75/2.67	3.02	279
tCzmPPC	2.80/2.82	2.77/2.70	2.97	339
SAcmPPC	2.68/2.73	2.73/2.68	2.79	334

Singlet energy determined at the onset point of the room temperature fluorescence spectra [a]in toluene solution and [b]of doped films (mCPCN: 10wt% emitter). Triplet energy determined at the onset of the low temperature phosphorescence spectra [c]in toluene solution and [d]of doped films. [e]The optical bandgap was determined from the onset point of absorption spectra. [f]Melting temperature.

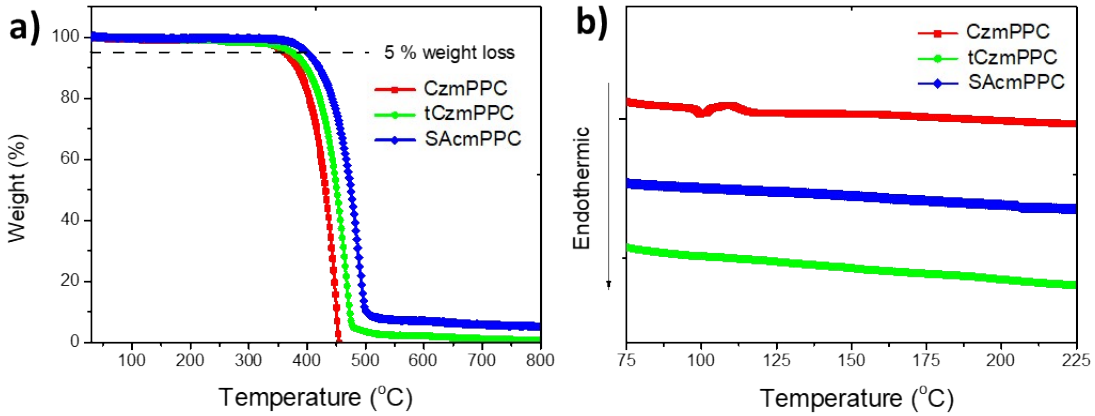

Figure S5. a) TGA curves and b) DSC curves of compounds CzmPPC, tCzmPPC, and SAcmPPC

Photoelectron spectral properties

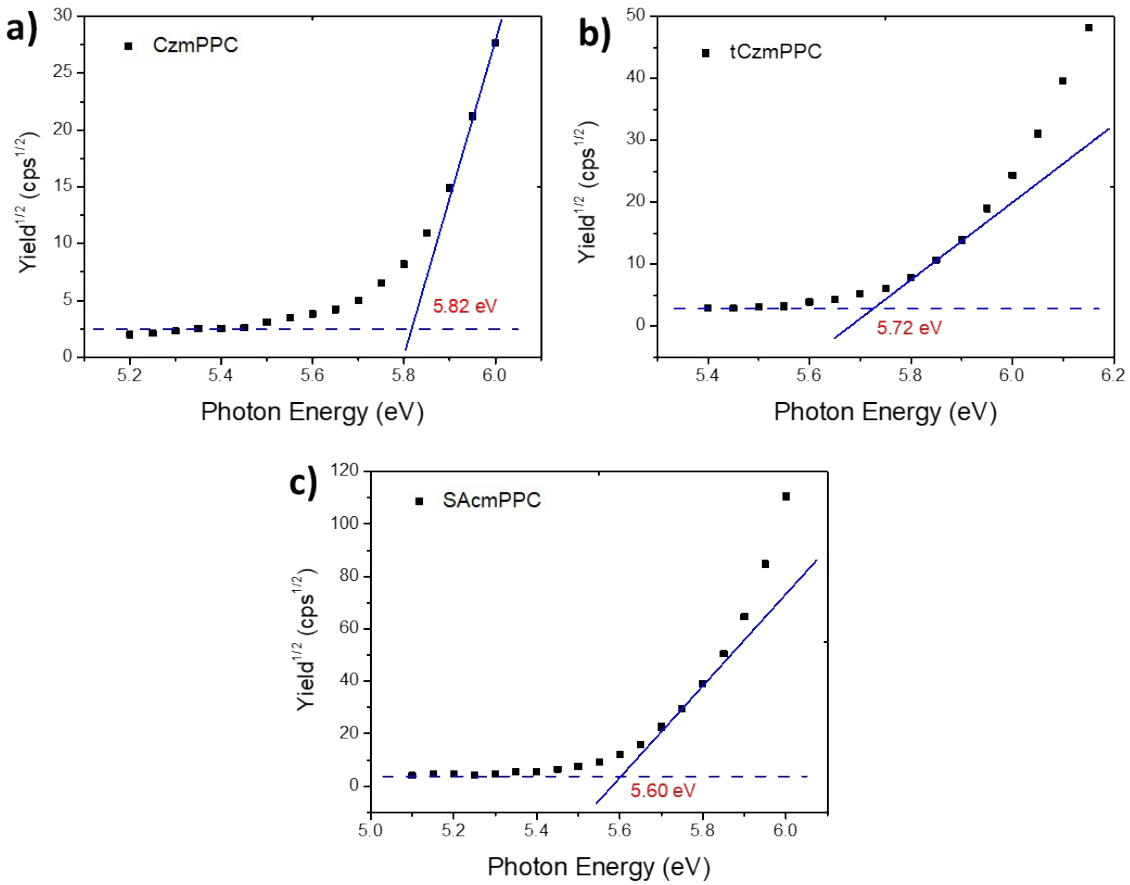

Figure S6. Photoelectron spectroscopy of neat film a) CzmPPC, b) tCzmPPC, and c) SAcmPPC.

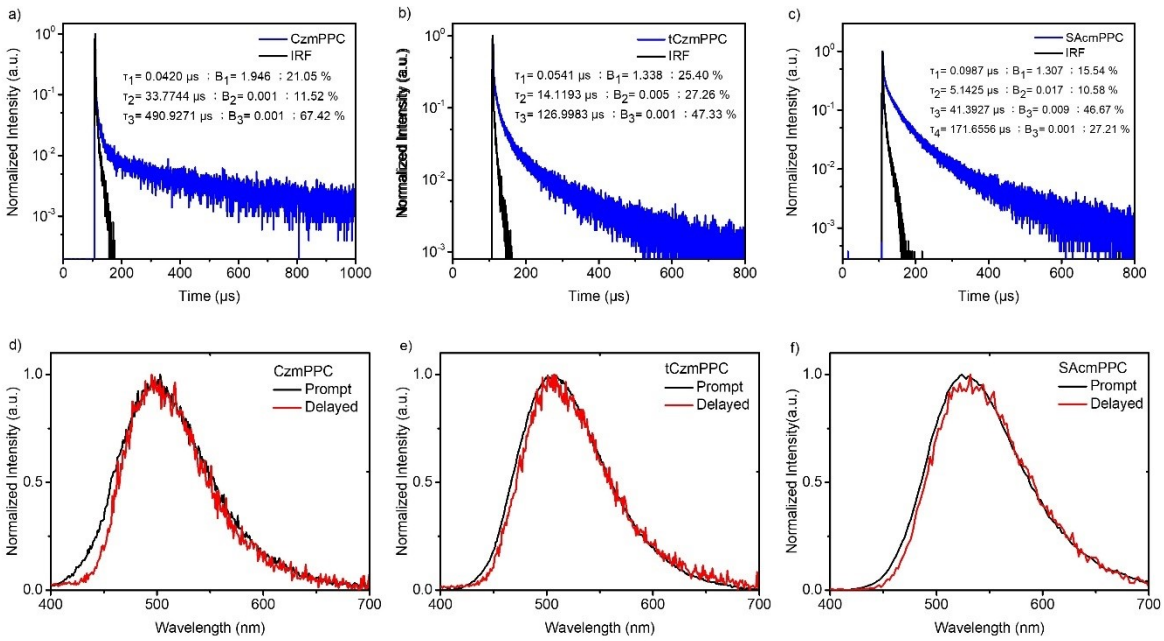

Figure S7. The prompt and delayed components in doped films (10% PPC compounds in mCPCN films) of a) CzmPPC, b) tCzmPPC, and c) SAcmPPC from time-resolved PL spectra. The prompt and delayed emission (gating time: 10 μs) spectra in doped films of d) CzmPPC, e) tCzmPPC, and f) SAcmPPC.

Table S5. Summarized transient-PL data and the rate constants of TADF dopants.

emitter[a]	ΔE_{ST} (eV)	τ_{PF} (ns)	τ_{DF} (μs)	Φ_P (%)	Φ_D (%)	k_r (10^6 s^{-1})[b]	k_{ISC} (10^7 s^{-1})[c]	k_{RISC} (10^4 s^{-1})[d]
CzmPPC	0.28	42.0	461.5	19.8	72.5	4.7	1.9	1.0
tCzmPPC	0.12	54.1	86.7	24.7	72.4	4.6	1.4	4.5
SAcmPPC	0.05	98.7	71.8	15.4	84.2	1.6	0.9	9.0

[a]10% PPC compounds measured in mCPCN film (20 nm) at 300 K. [b] Rate constant of fluorescence radiative decay: $k_r = \Phi_P/\tau_{PF}$. [c] Rate constant of ISC: $k_{ISC} = (1-\Phi_P)/\tau_{PF}$. [d] Rate constant of RISC: $k_{RISC} = \tau_{DF}/(k_{ISC}\cdot\tau_{PF}\cdot\tau_{DF}\cdot\Phi_P)$.

Table S6. Fitting results[a] of transient-PL.

emitter[b]	$\tau_1 = \tau_{PF}$ (μs)	B_1 (value)	τ_2 (μs)	B_2 (value)	τ_3 (μs)	B_3 (value)	τ_4 (μs)	B_4 (value)	τ_{av} [c] $= \tau_{DF}$ (μs)
CzmPPC	42.0	1.946	33.8	0.001	490.9	0.001	-	-	461.5
tCzmPPC	54.1	1.338	14.1	0.005	127.0	0.001	-	-	86.7
SAcmPPC	98.7	1.307	5.1	0.017	41.4	0.009	171.7	0.001	71.8

[a]Fitting method: $R(t) = B_1 e^{(-t/\tau_1)} + B_2 e^{(-t/\tau_2)} + B_3 e^{(-t/\tau_3)} + B_4 e^{(-t/\tau_4)}$. [b]10% PPC compounds measured in mCPCN film (20 nm) at 300 K. [c]$\tau_{av} = \frac{[\sum B_i \tau_i^2]}{[\sum B_i \tau_i]}$, where B_1 and τ_1 are not included.

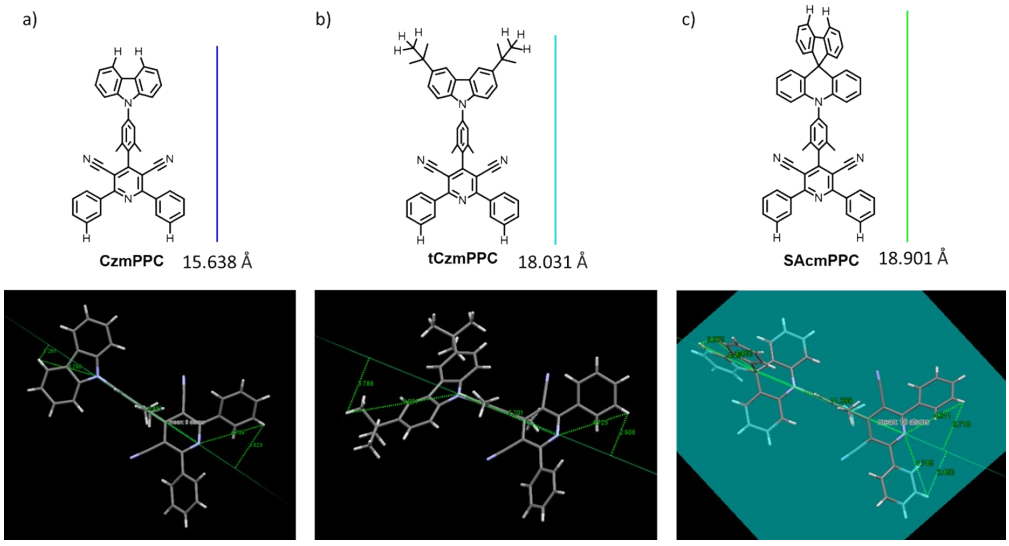

Figure S8. Molecular lengths from XRD for a) CzmPPC, b) tCzmPPC, and c) SAcmPPC, respectively. We measured the lenghs from the distance of horizontal projection of outside hydrogen atoms to the central xylene plane.

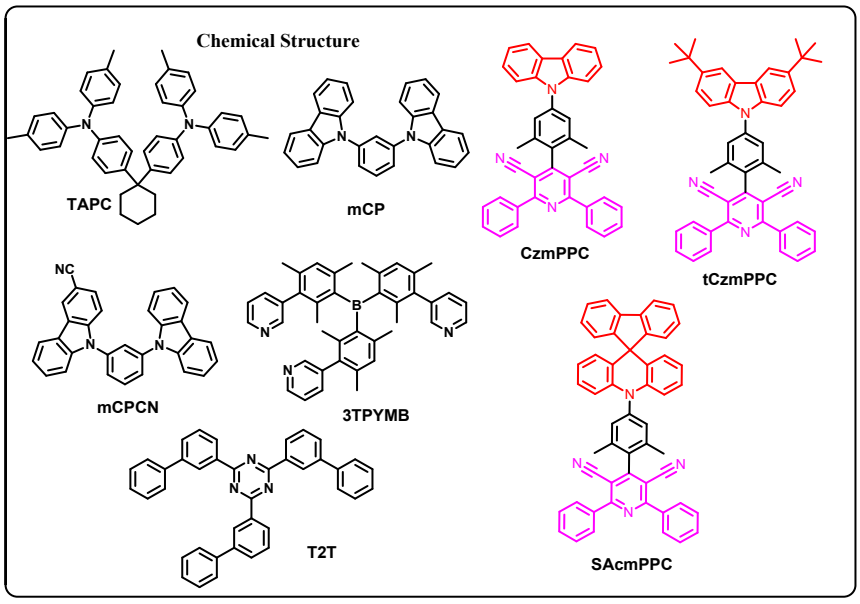

Figure S9. Chemical structures of the materials used in the device fabrication.

References

[1] A.V. Krukau, O.A. Vydrov, A.F. Izmaylov, G.E. Scuseria, Influence of the exchange screening parameter on the performance of screened hybrid functionals, J. Chem. Phys 125 (2006) 224106.
[2] S. Grimme, J. Antony, S. Ehrlich, H. Krieg, A consistent and accurate ab initio parametrization of density functional dispersion correction (DFT-D) for the 94 elements H-Pu, J. Chem. Phys 132 (2010) 154104.

^{1}H and ^{13}C NMR spectra of 4-(9*H*-carbazol-9-yl)-2,6-dimethylbenzaldehyde.

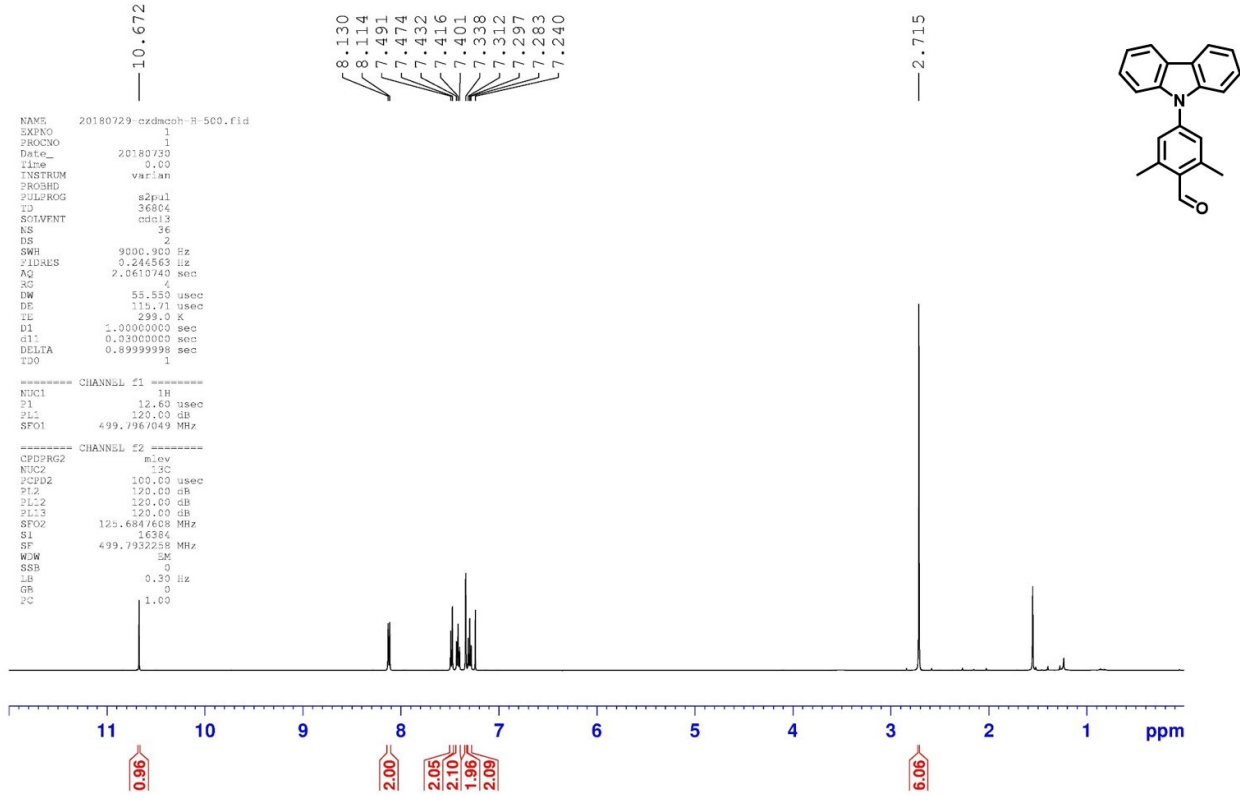

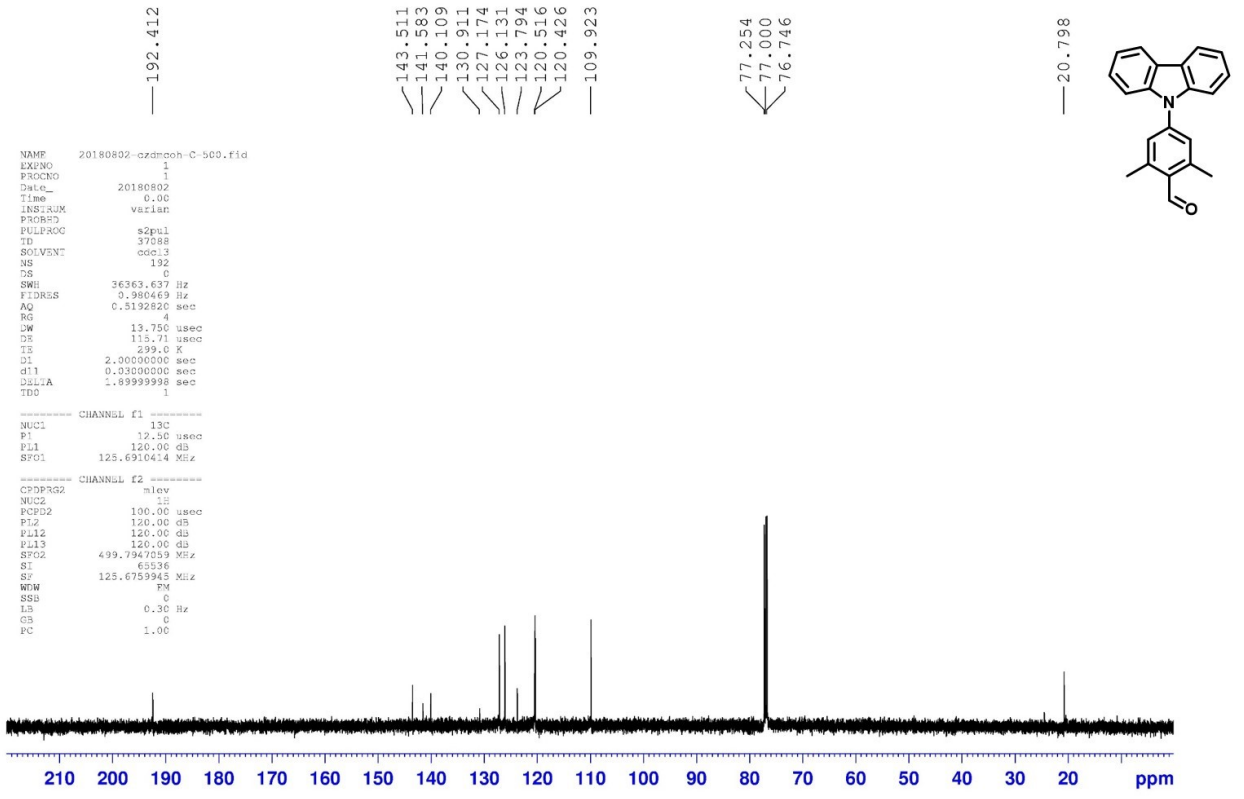

^{1}H and ^{13}C NMR spectra of 4-(3,6-di-*tert*-butyl-9*H*-carbazol-9-yl)-2,6-dimethylbenzaldehyde.

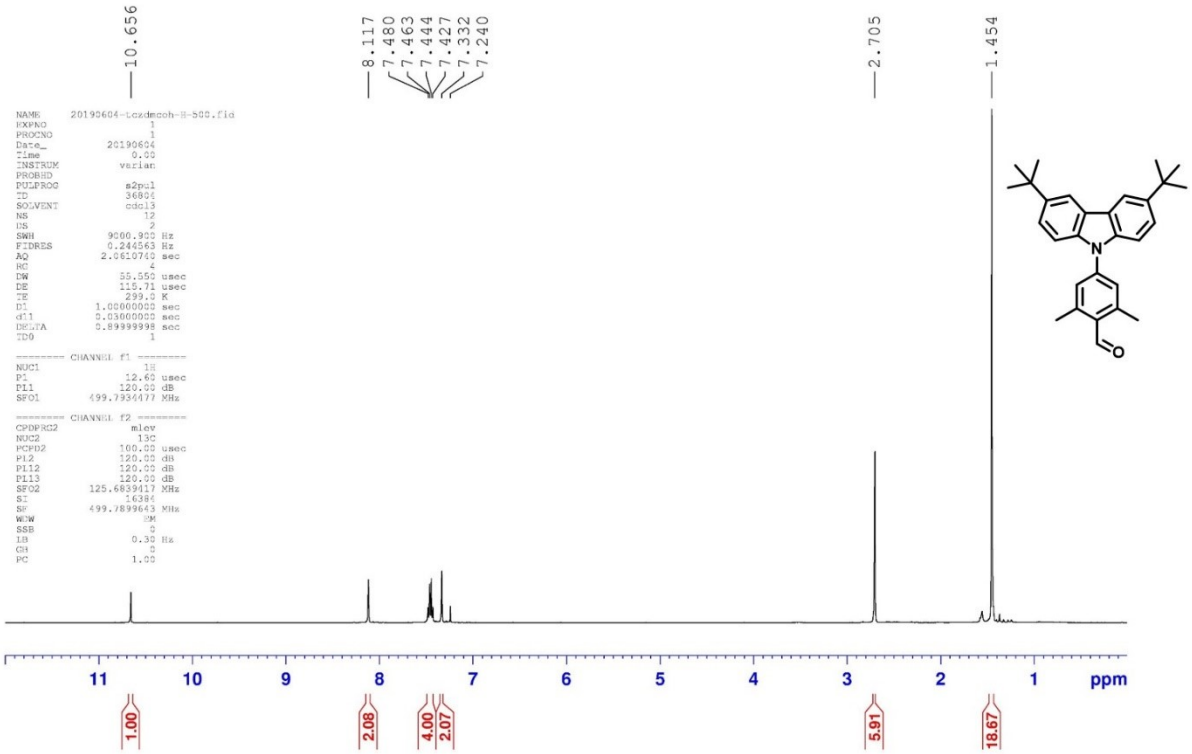

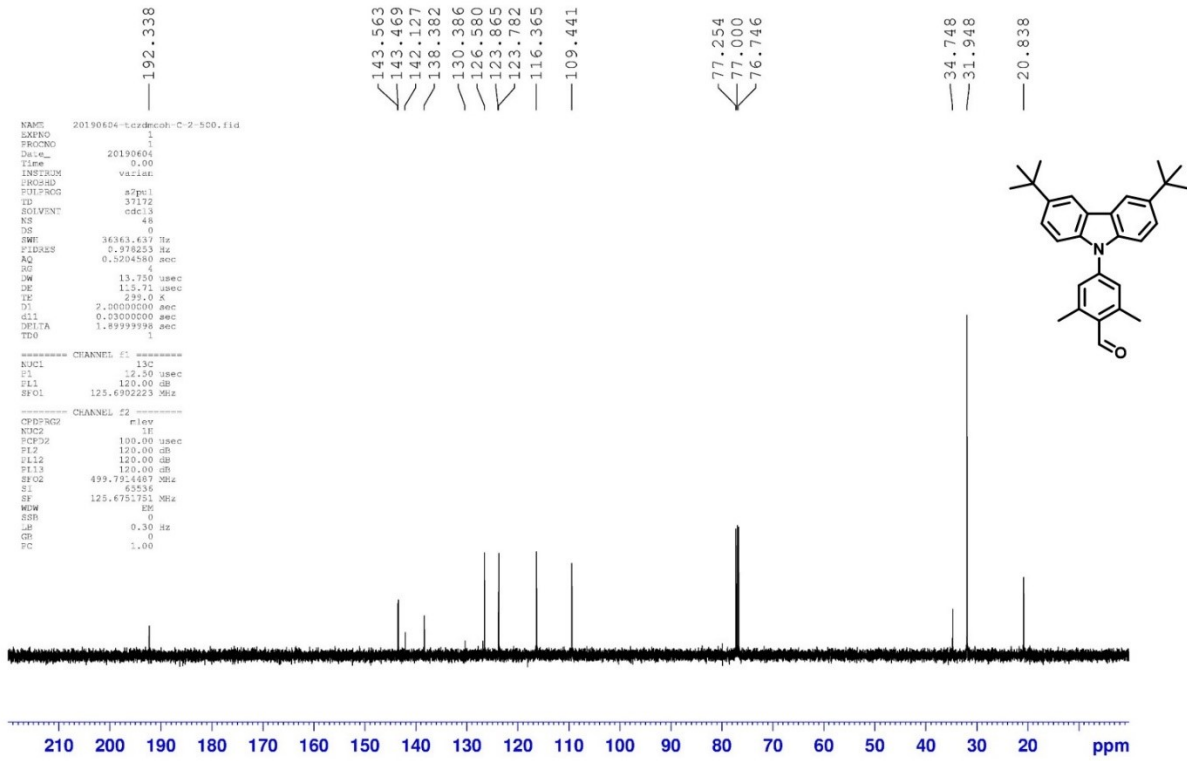

^{1}H and ^{13}C NMR spectra of 2,6-dimethyl-4-(10*H*-spiro[acridine-9,9'-fluoren]-10-yl)benzaldehyde.

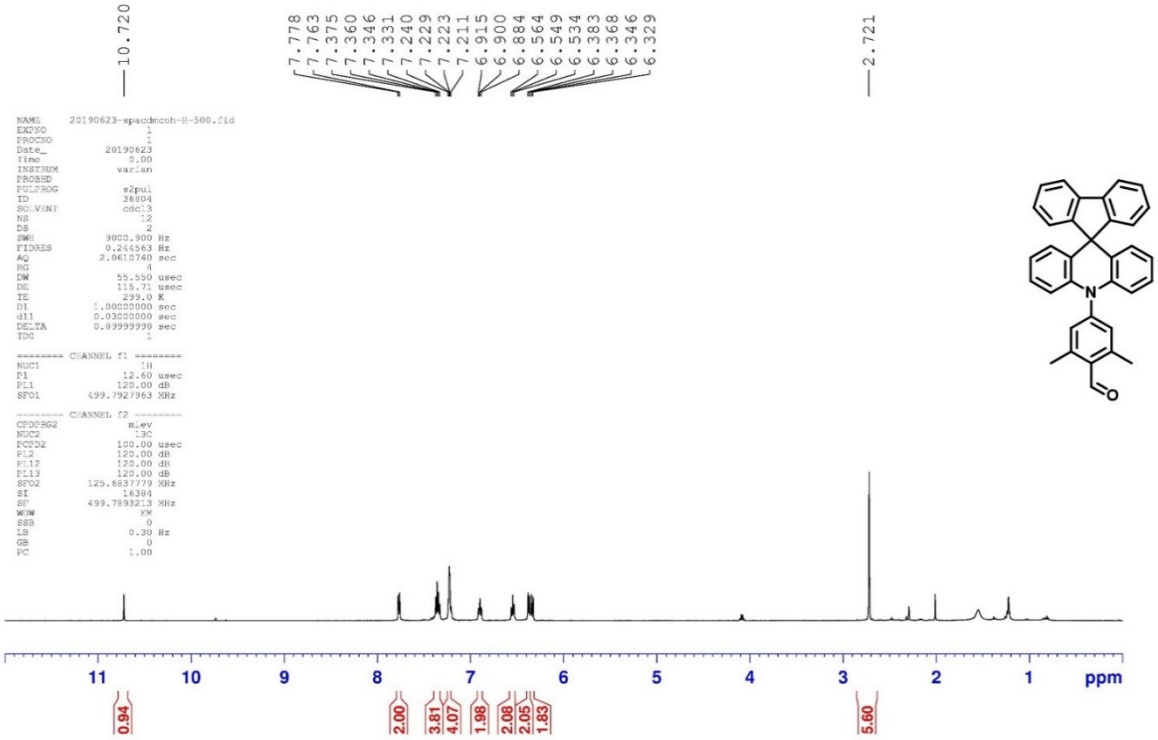

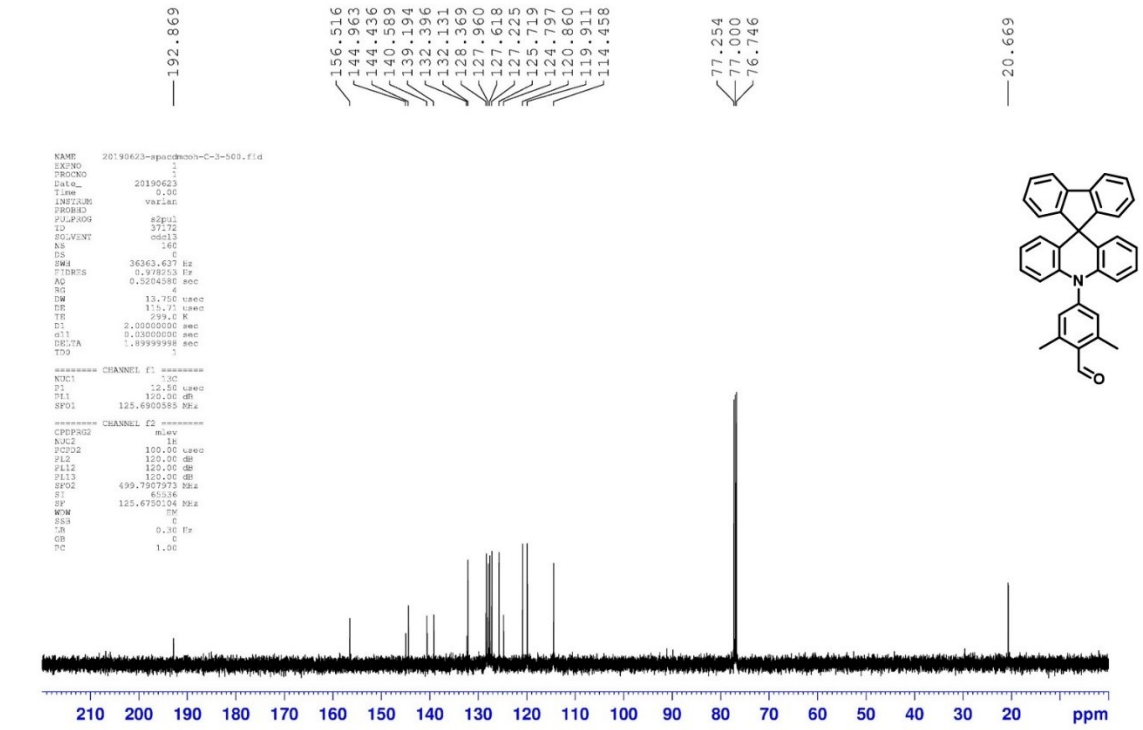

^{1}H and ^{13}C NMR spectra of 4-(4-(9*H*-carbazol-9-yl)-2,6-dimethylphenyl)-2,6-diphenylpyridine-3,5-dicarbonitrile (CzmPPC).

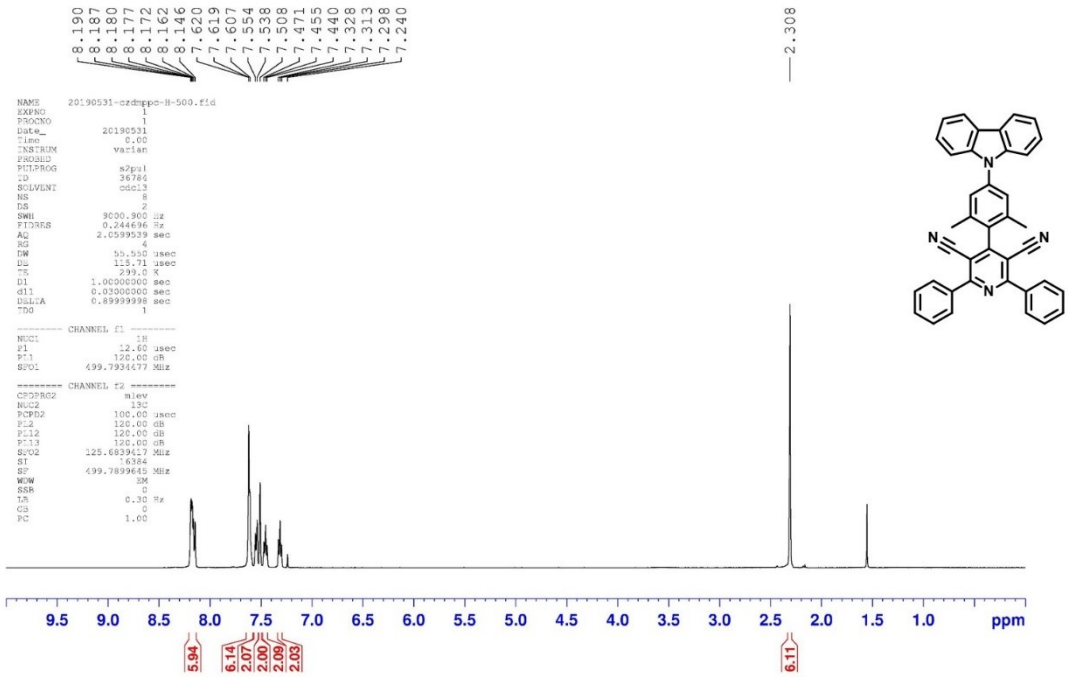

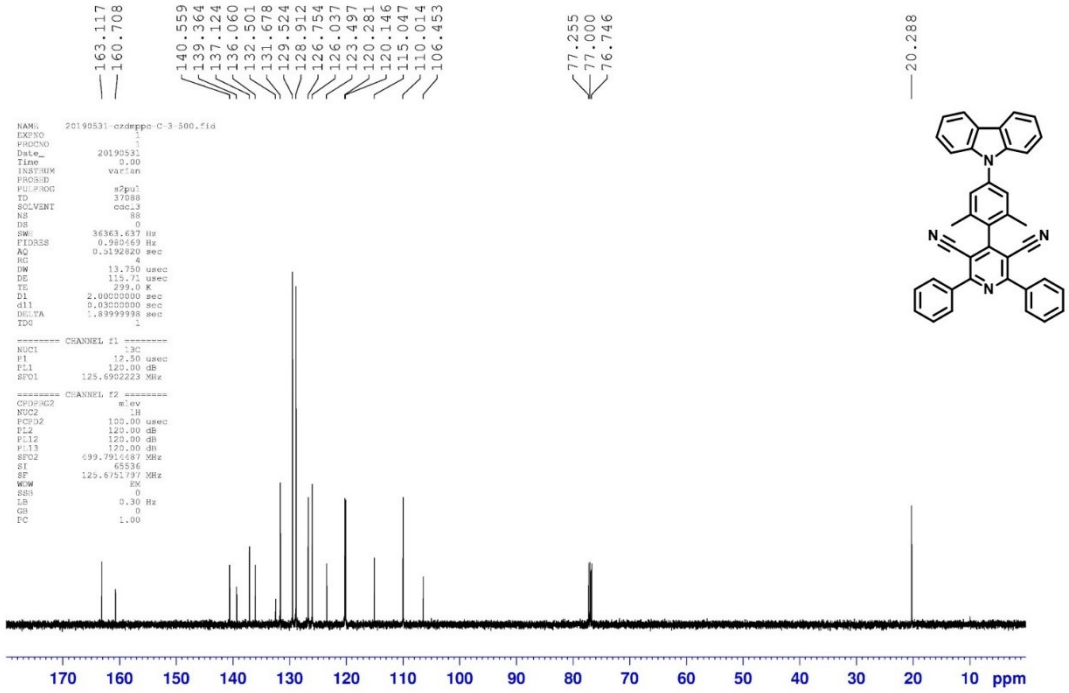

^{1}H and ^{13}C NMR spectra of 4-(4-(3,6-di-tert-butyl-9*H*-carbazol-9-yl)-2,6-dimethylphenyl)-2,6-diphenylpyridine-3,5-dicarbonitrile (tCzmPPC).

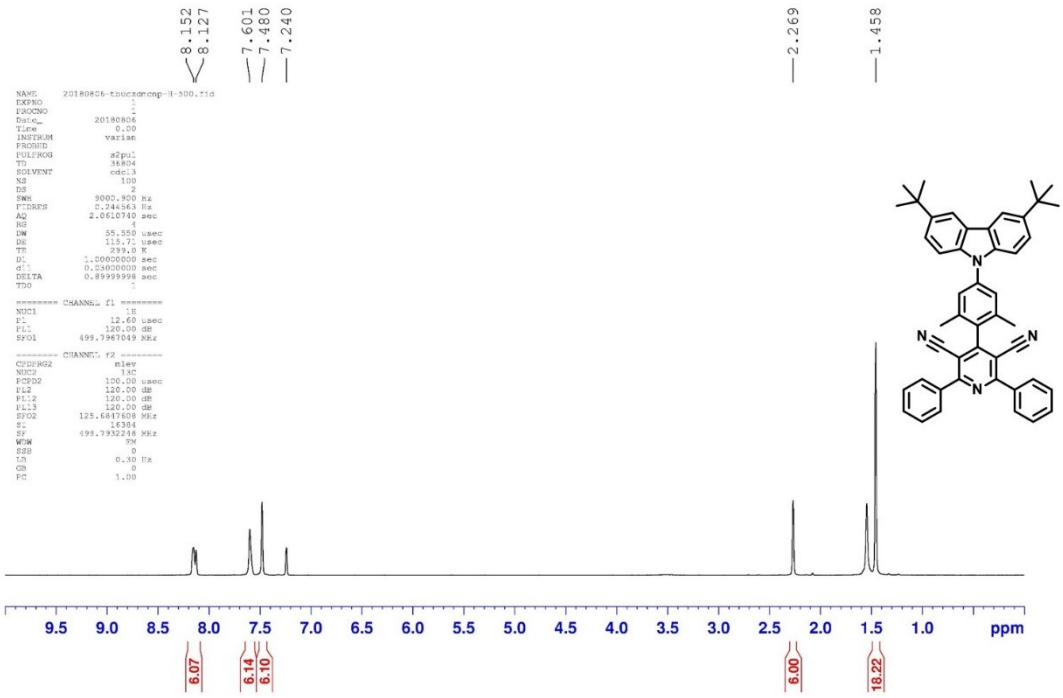

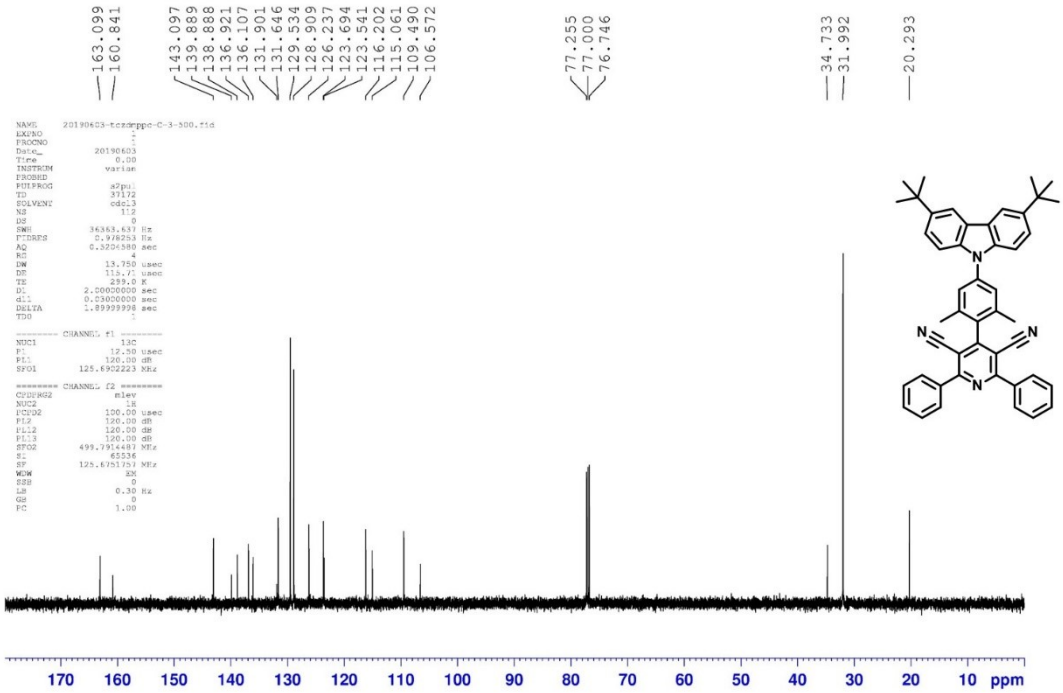

^{1}H and ^{13}C NMR spectra of 4-(2,6-dimethyl-4-(10*H*-spiro[acridine-9,9'-fluoren]-10-yl)phenyl)-2,6-diphenylpyridine-3,5-dicarbonitrile (SAcmPPC).

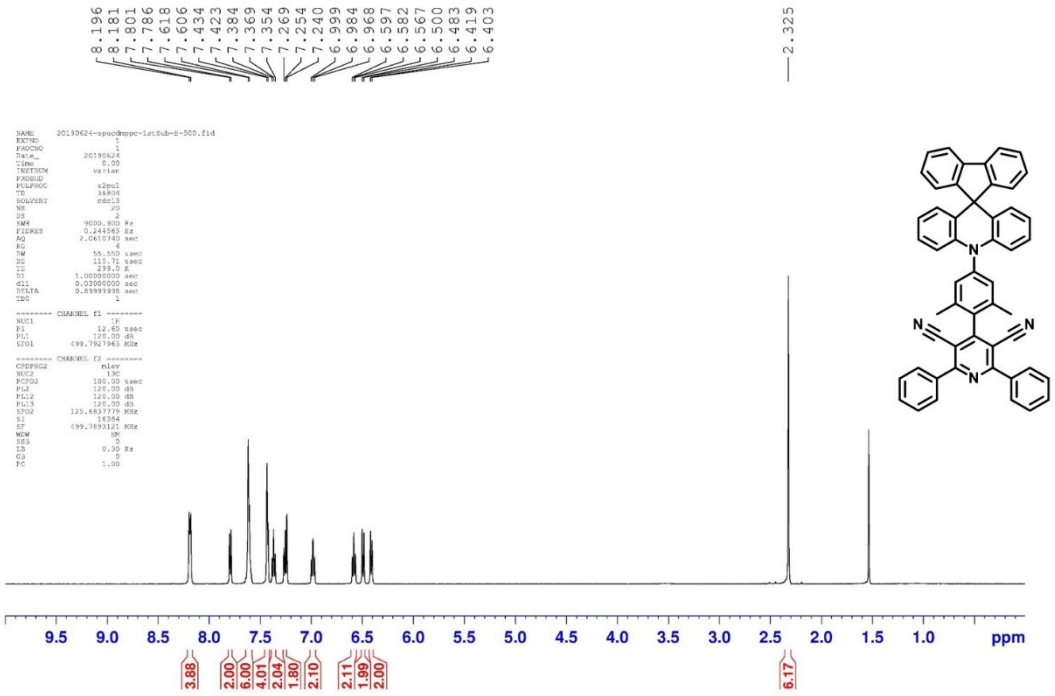

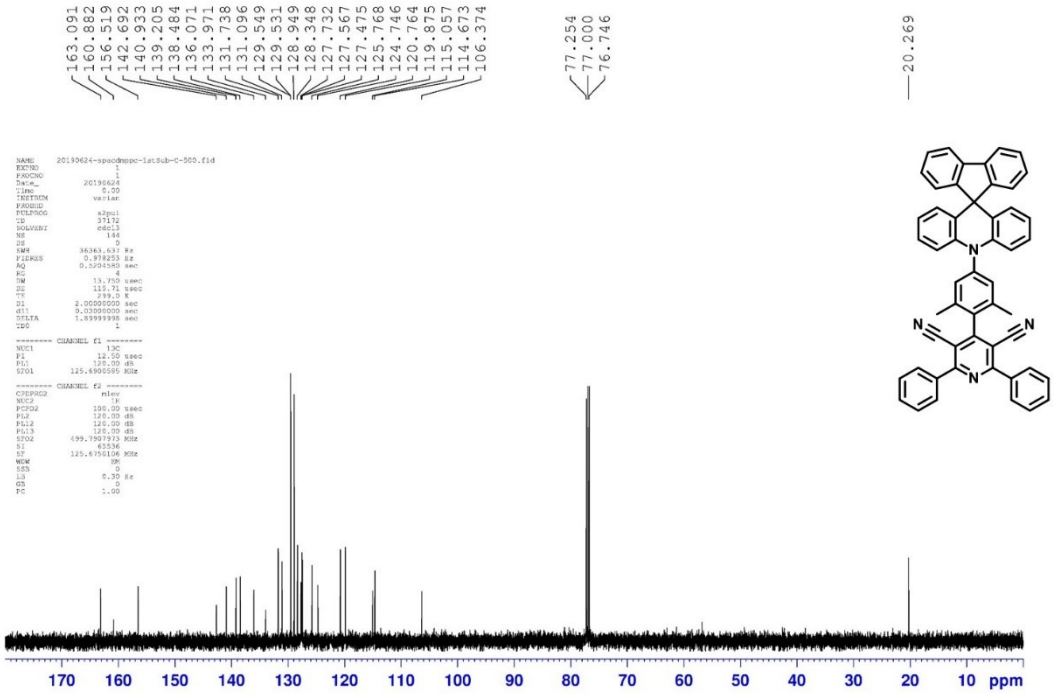

X-ray crystallographic analysis:

General Crystal Growing Conditions: X-ray quality single crystals of **CzmPPC, tCzmPPC** and **SAcmPPC,** were collected from the sublimed tube after cooling down to room temperature (heated at various temperatures by slow evaporation under pressure).

ORTEP diagram of compound **CzmPPC (**CCDC 2144158)

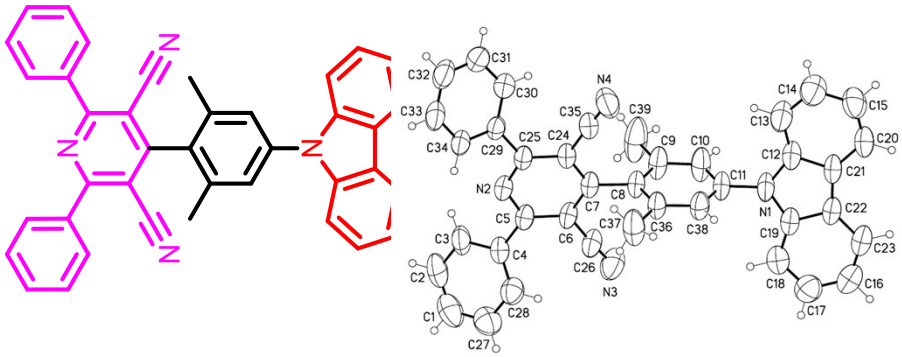

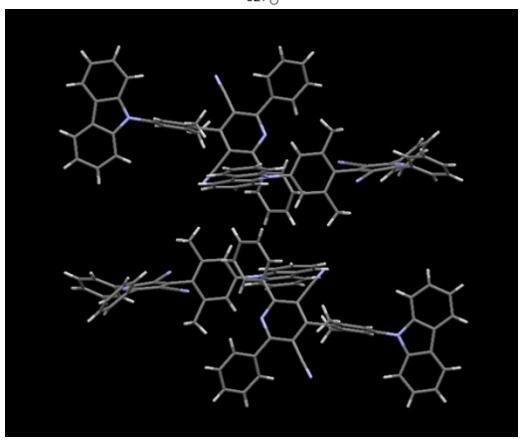

Table S5. Crystal data and structure refinement for 190441lt_a_pl.

Identification code	190441lt_a_pl	
Empirical formula	C37 H24 N4	
Formula weight	524.60	
Temperature	296(2) K	
Wavelength	0.71073 Å	
Crystal system	Monoclinic	
Space group	I2/a	
Unit cell dimensions	a = 8.5539(5) Å	□= 90°.

	b = 16.6478(9) Å □= 90.721(4)°.
	c = 18.5307(10) Å □ = 90°.
Volume	2638.6(3) $Å^3$
Z	4
Density (calculated)	1.321 Mg/m^3
Absorption coefficient	0.079 mm^{-1}
F(000)	1096
Crystal size	0.22 x 0.20 x 0.20 mm^3
Theta range for data collection	1.644 to 26.692°.
Index ranges	-10<=h<=10, -20<=k<=20, -23<=l<=23
Reflections collected	20090
Independent reflections	2744 [R(int) = 0.0376]
Completeness to theta = 25.242°	100.0 %
Absorption correction	Semi-empirical from equivalents
Max. and min. transmission	0.7454 and 0.6739
Refinement method	Full-matrix least-squares on F^2
Data / restraints / parameters	2744 / 0 / 188
Goodness-of-fit on F^2	1.102
Final R indices [I>2sigma(I)]	R1 = 0.0529, wR2 = 0.1237
R indices (all data)	R1 = 0.0607, wR2 = 0.1292
Extinction coefficient	n/a
Largest diff. peak and hole	0.220 and -0.230 $e.Å^{-3}$

ORTEP diagram of compound **tCzmPPC (**CCDC 2144160)

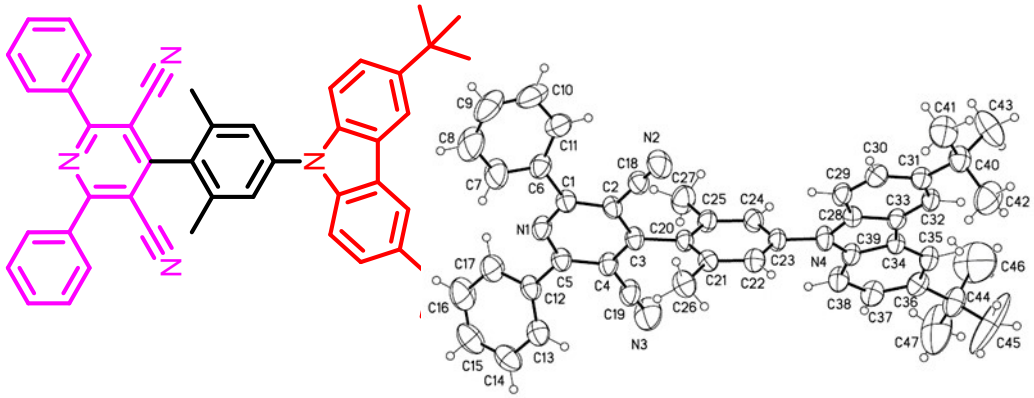

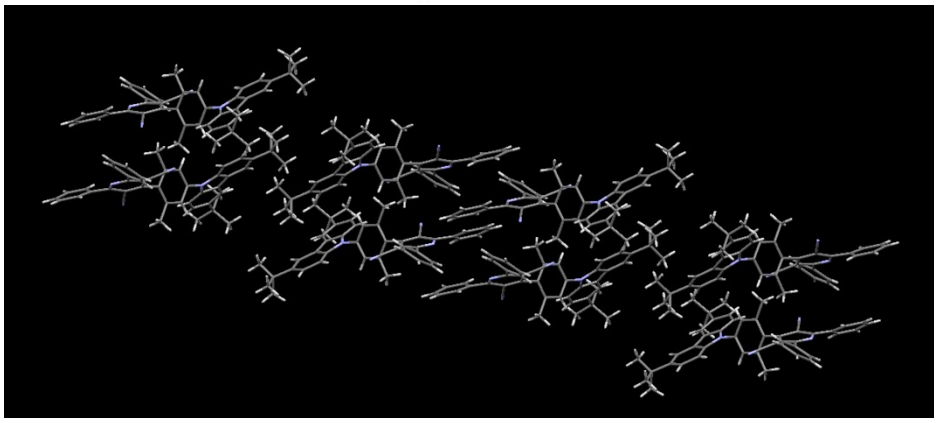

Table S6. Crystal data and structure refinement for 190122lt_0m.

Identification code	190122LT_0m	
Empirical formula	C39 H28 N4	
Formula weight	552.65	
Temperature	100(2) K	
Wavelength	0.71073 Å	
Crystal system	Monoclinic	
Space group	P 21/c	
Unit cell dimensions	a = 11.3340(8) Å	□= 90°.
	b = 22.7417(15) Å	□= 96.470(4)°.
	c = 11.3907(8) Å	□ = 90°.
Volume	2917.3(3) Å^3	
Z	4	
Density (calculated)	1.258 Mg/m^3	
Absorption coefficient	0.075 mm^{-1}	

F(000)	1160
Crystal size	0.10 x 0.08 x 0.07 mm^3
Theta range for data collection	1.791 to 26.444°.
Index ranges	-14<=h<=14, -28<=k<=28, -14<=l<=14
Reflections collected	48452
Independent reflections	5987 [R(int) = 0.0415]
Completeness to theta = 25.242°	100.0 %
Absorption correction	Semi-empirical from equivalents
Max. and min. transmission	0.7454 and 0.6766
Refinement method	Full-matrix least-squares on F^2
Data / restraints / parameters	5987 / 0 / 390
Goodness-of-fit on F^2	1.016
Final R indices [I>2sigma(I)]	R1 = 0.0395, wR2 = 0.0886
R indices (all data)	R1 = 0.0530, wR2 = 0.0950
Extinction coefficient	n/a
Largest diff. peak and hole	0.215 and -0.181 e.$Å^{-3}$

ORTEP diagram of compound **SAcmPPC (**CCDC 2144159)

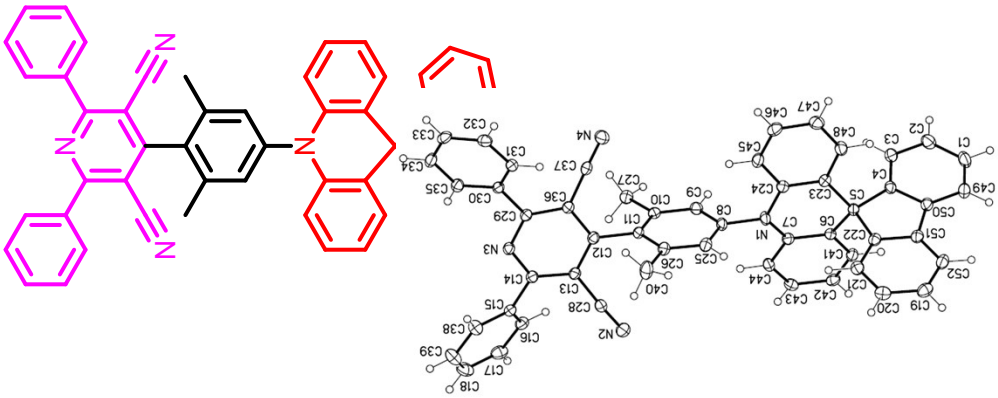

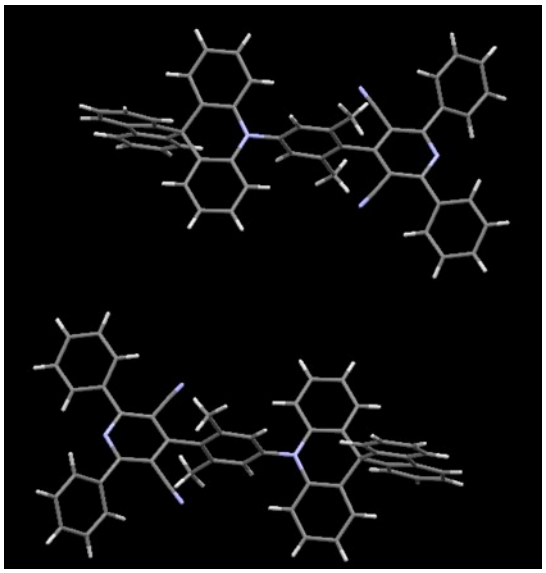

Table S7. Crystal data and structure refinement for mo_191021lt_0m.

Identification code	mo_191021LT_0m	
Empirical formula	C47 H44 N4	
Formula weight	664.86	
Temperature	100(2) K	
Wavelength	0.71073 Å	
Crystal system	Monoclinic	
Space group	$P2_1/n$	
Unit cell dimensions	a = 18.9196(19) Å	□= 90°.
	b = 8.7386(8) Å	□= 112.002(3)°.
	c = 24.498(2) Å	□ = 90°.
Volume	3755.4(6) $Å^3$	
Z	4	
Density (calculated)	1.176 Mg/m^3	
Absorption coefficient	0.069 mm^{-1}	
F(000)	1416	
Crystal size	0.12 x 0.03 x 0.03 mm^3	
Theta range for data collection	1.171 to 26.559°.	
Index ranges	-22<=h<=23, -10<=k<=11, -30<=l<=30	
Reflections collected	55347	
Independent reflections	7462 [R(int) = 0.1597]	
Completeness to theta = 25.242°	96.4 %	

Absorption correction	Semi-empirical from equivalents
Max. and min. transmission	0.7454 and 0.5995
Refinement method	Full-matrix least-squares on F^2
Data / restraints / parameters	7462 / 0 / 469
Goodness-of-fit on F^2	1.097
Final R indices [I>2sigma(I)]	R1 = 0.0979, wR2 = 0.2379
R indices (all data)	R1 = 0.1673, wR2 = 0.2690
Extinction coefficient	0.0059(10)
Largest diff. peak and hole	0.597 and -0.323 e.$Å^{-3}$

Mass spectra of TADF emitters

CzmPPC

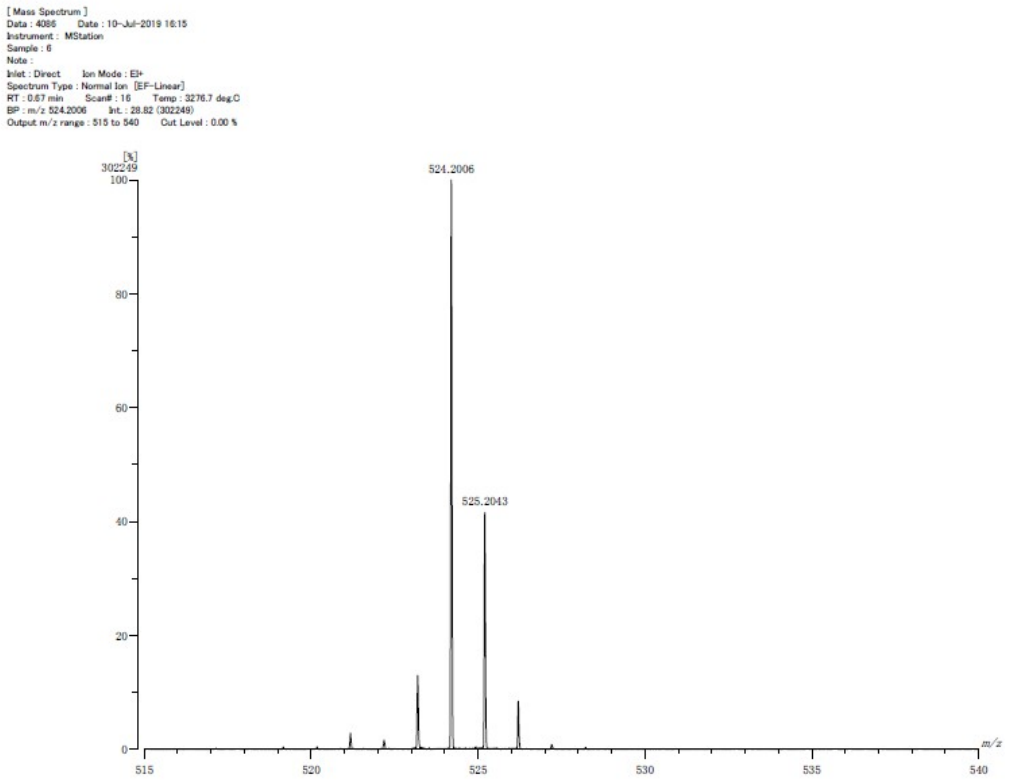

tCzmPPC

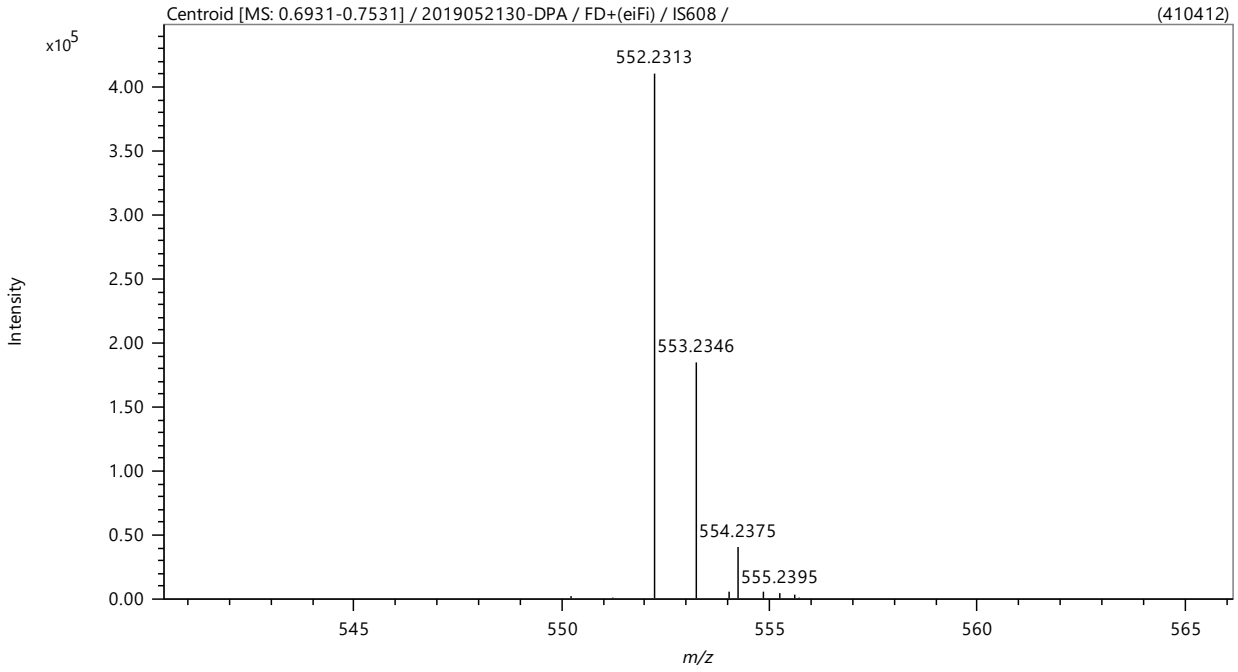

SAcmPPC

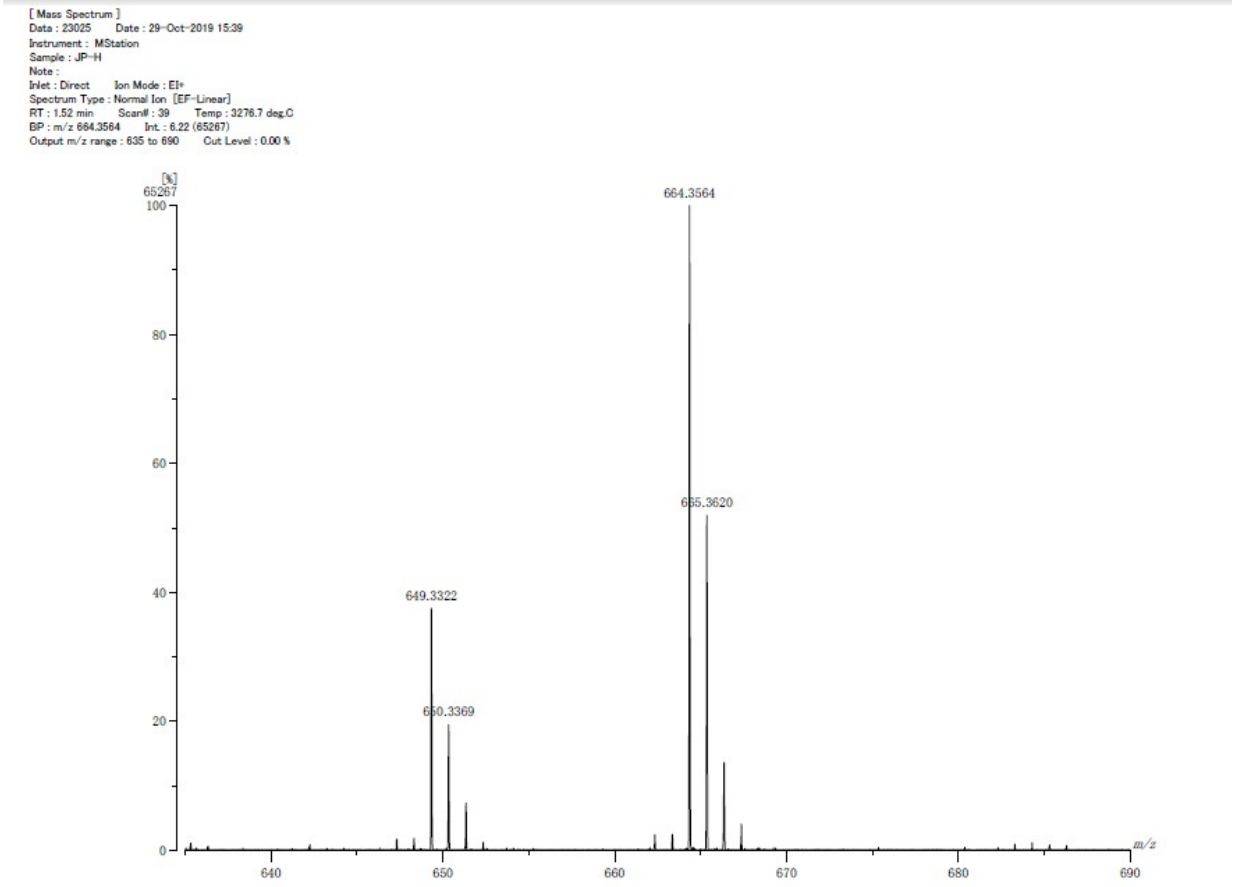

1. A. V. Krukau, O. A. Vydrov, A. F. Izmaylov and G. E. Scuseria, *J Chem Phys*, 2006, **125**, 224106.
2. S. Grimme, J. Antony, S. Ehrlich and H. Krieg, *J Chem Phys*, 2010, **132**, 154104.